Dalton Transactions

ROYAL SOCIETY OF CHEMISTRY

PAPER

View Article Online
View Journal | View Issue

Check for updates

Cite this: *Dalton Trans.*, 2026, **55**, 1490

# Symmetry and substituent electronics dictate electronic structure of low spin, mixed-ring rhenocene complexes

Eyram Asempa, †[a] Gregory M. Curtin, †[a,b] Ann Marie May, †[b] Jillian L. Dempsey *[b] and Elena Jakubikova *[a]

Identifying the impact of molecular structure and symmetry on excited state character and energetics is vital to enable and control photochemical reactions. In this work, density functional theory (DFT) and time-dependent DFT (TD-DFT) were used to determine the electronic structure and excited state reduction potentials of six heteroleptic rhenocene complexes, each bearing a cyclopentadienyl ligand and a functionalized tetramethylated cyclopentadienyl ligand (ReCp(CpMe$_4$R), where Me = $CH_3$ and R = Me, $CF_3$, $^t$Bu, $CHCH_2$, CHO, or OMe). Calculations were performed using the B3LYP and BP86 functionals, utilizing SDD + f effective core potential and its associated basis set for Re, and 6-311G* basis set for all other atoms. All six complexes exhibit eclipsed geometries with similar Re-ring bond distances and angles. Despite their structural similarities, the electronic structure of these complexes varies with ligand functionalization. ReCp(Cp*), **1**, (where Cp* = pentamethylcyclopentadienyl) has a $^2A_1$ ground state with a $d_{z^2}$-based LUMOβ orbital, whereas functionalized tetramethylated derivatives, **2–6**, have $^2A''$ ground states with $d_{x^2-y^2}$-based LUMOβ orbitals due to their lower molecular symmetries ($C_{5v}$ *vs.* $C_s$, respectively). Regardless, complementary TD-DFT and fragment orbital analyses show that low-energy LMCT excited states are retained across all six complexes (where LMCT character > 90%). Furthermore, hypsochromic shifts and higher oscillator strengths are observed for **2–6** compared to **1**, resulting from the changes in HOMO$\beta$–LUMO$\beta$ gaps and excitation into the $d_{x^2-y^2}$ orbital for **2–6** rather than $d_{z^2}$ orbital for **1**, which increases the orbital overlap between the hole–particle pairs that describe the lowest-energy LMCT excitations. Appending electron donating and withdrawing groups to these mixed-ring rhenocene derivatives also tunes ground state and excited state reduction potentials over a 400 mV and 700 mV range, respectively, enabling access to more oxidizing LMCT excited states. Collectively, these results showcase design strategies to control acceptor orbital character, orbital energetics, excited state energies, and reduction potentials, while simultaneously retaining low-energy LMCT excited states across a series of rhenocene derivatives. In result, this work establishes approaches to design and tailor next-generation mixed-ring rhenocenes with low-energy LMCT excited states for photochemical applications.

Received 26th November 2024,
Accepted 16th December 2025

DOI: 10.1039/d4dt03309d

rsc.li/dalton

Open Access Article. Published on 22 December 2025. Downloaded on 6/9/2026 9:34:24 AM.
This article is licensed under a Creative Commons Attribution-NonCommercial 3.0 Unported Licence.

## Introduction

An array of photochemical reactions are known for metallocene complexes, including photopolymerizations, photoisomerizations, and excited state electron transfer reactions.[1–9] For example, ferrocene and other Group VIII metallocenes are well known to generate ground state adducts with solvent and upon irradiation undergo charge transfer to solvent, generating radical species that trigger a wide range of polymerization reactions.[1,2] Other metallocenes, such as cobaltocene and benzoyl-substituted ferrocene derivatives, are known to undergo ligand loss *via* bond homolysis or ligand dissociation, where expelled ligands catalyze [2 + 2 + 2] cyclotrimerizations or initiate anionic polymerizations, respectively.[2,3] This observed photoreactivity is largely dictated by the nature of the metallocene's excited state (*e.g.*, d–d, ligand-to-metal charge transfer (LMCT), metal-to-ligand charge transfer (MLCT), and/or charge transfer-to-solvent (CTTS) character) and the excited state energetics. Therefore, understanding the nature of the donor and acceptor orbitals of these photoactive excited state transitions is valuable in understanding and predicting accessible photochemical reactions. Similarly, identifying strategies to manipulate the character of these orbitals and enable control of orbital energetics and absorption energies is also

[a]*Department of Chemistry, North Carolina State University, Raleigh, NC 27695, USA. E-mail: ejakubi@ncsu.edu*
[b]*Department of Chemistry, University of North Carolina at Chapel Hill, Chapel Hill, NC 27514, USA. E-mail: dempseyj@email.unc.edu*
† These authors contributed equally.


This journal is © The Royal Society of Chemistry 2026

Open Access Article. Published on 22 December 2025. Downloaded on 6/9/2026 9:34:24 AM.
This article is licensed under a Creative Commons Attribution-NonCommercial 3.0 Unported Licence.

vital for tuning the photochemical reactivity of metallocenes. For example, previous studies by Malischewski and co-workers[10] have shown that the substitution of cyclopentadienyl ligands with electron-withdrawing groups influences the metal–ligand bonding energies of several transition metal complexes.[11] As such, these synthetic modifications afford control over molecular orbital energies and in turn, also influence their oxidative and reductive properties.

Recently, we reported on the electronic structure and photophysics of two metallocenes: decamethylmanganocene ($MnCp^*_2$) and decamethylrhenocene ($ReCp^*_2$).[12] Both low spin $d^5$ complexes were interrogated using time-dependent density functional theory (TD-DFT), and these calculations support that both complexes have low energy LMCT excited states. These excited states result from the donation of electrons from orbitals delocalized across both pentamethylcyclopentadienyl (Cp*) ligands to the metal $d_{x^2-y^2}$ orbitals upon illumination. Both complexes exhibit strongly reducing excited states with excited state reduction potentials of −3.38 V and −2.61 *vs.* $Fc^{+/0}$ for the $Mn^{III/II*}$ and $Re^{III/II*}$ couples, respectively.[12] Conversely, their LMCT excited states are only mildly oxidizing with modest reduction potentials for their $Mn^{II*/I}$ and $Re^{II*/I}$ redox couples (−0.18 V and −0.20 V *vs.* $Fc^{+/0}$, respectively). In addition, $ReCp^*_2$ exhibits room temperature photoluminescence upon excitation of the LMCT band with a 1.8 ns lifetime,[12,13] while $MnCp^*_2$ is not photoluminescent at room temperature. These results suggest that $ReCp^*_2$ is a promising candidate to participate in excited state electron transfer reactions. However, further exploration is limited largely due to the difficult synthesis of $ReCp^*_2$ which requires specialized instrumentation and energy intensive protocols. Currently, the only known synthetic route requires the vaporization of rhenium metal using electron beam evaporation and co-condensation with pentamethylcyclopentadiene to yield decamethylrhenocene hydride, $HReCp^*_2$.[14,15] Subsequent UV photolysis yields $ReCp^*_2$.[16]

Given the complexity of decamethylrhenocene's synthesis, targeting easier-to-synthesize rhenocene derivatives is advantageous. Notably, a mixed sandwich rhenium hydride, HReCp*Cp, has been previously synthesized and we hypothesize analogous photolyses may enable access to other rhenocene analogues with electronic structures similar to $ReCp^*_2$.[16,17] Therefore, we aimed to computationally study the electronic structure of (pentamethylcyclopentadienyl)(cyclopentadienyl)rhenium(II) (ReCpCp*, **1**), explore the nature of its excited states, and visualize the donor and acceptor orbitals that comprise its low energy electronic transitions. Furthermore, five derivatives, (1-trifluoromethyl-2,3,4,5-tetramethylcyclopentadienyl)(cyclopentadienyl)rhenium(II) (**2**) (1-*tert*-butyl-2,3,4,5-tetramethylcyclopentadienyl)(cyclopentadienyl)rhenium (II) (**3**), (1-vinyl-2,3,4,5-tetramethylcyclopentadienyl)(cyclopentadienyl)rhenium(II) (**4**), (1-formyl-2,3,4,5-tetramethylcyclopentadienyl)(cyclopentadienyl)rhenium(II) (**5**) and (1-methoxy-2,3,4,5-tetramethylcyclopentadienyl)(cyclopentadienyl)rhenium(II) (**6**) were also explored (Fig. 1), as synthetic precedence is known for their asymmetric cyclopentadienyl ligands, with the exception of the methoxy derivative.[18–20] Investigating these derivatives with substituted cyclopentadienyl rings also revealed the impact of steric encumbrance, ligand donor strength, and molecular symmetry on excited state energies, excited state character, and their relative orbital ordering. Likewise, the impact of ligand functionalization on ground and excited state reduction potentials ($E^\circ$ and $E^{\circ*}$, respectively) was also explored, showcasing synthetic strategies to tune the potency of the LMCT excited states to drive photooxidative reactions. From this approach, this study serves to provide insight into the electronic structure and nature of the low energy LMCT excited states of heteroleptic rhenocene derivatives and aid in the synthetic development of next-generation monomeric rhenocene complexes for photosensitization reactions.

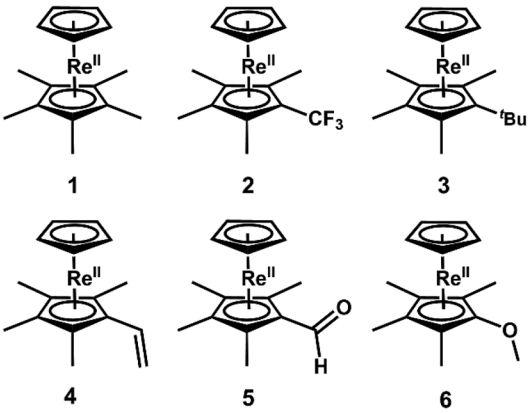


**Fig. 1** Re(Cp)(CpMe$_4$R) complexes where R = Me, $CF_3$, $^t$Bu, $CHCH_2$, CHO, or OMe.

## Methodology

All metallocenes (**1**–**6**) were optimized in doublet, quartet, and sextet states using the UB3LYP[21,22] functional with Grimme's D3 dispersion correction.[23] The SDD basis sets with effective core potentials and an additional f polarization function were used for Re[24,25] while the 6-311G* basis set was employed for all other atoms (H, C, F, O).[26,27] This methodology was selected due to its precedence in describing the ground and excited state structure of other low spin, $d^5$ metallocenes.[12] Geometry optimizations were performed on all structures in benzene as the implicit solvation model *via* a polarizable continuum model (PCM).[28] Vibrational frequency calculations were performed to ensure that all optimized structures were true minima with no imaginary frequencies. Time-dependent density functional theory (TD-DFT)[29] was employed to calculate the ultraviolet-visible (UV-Vis) absorption spectra for each complex, using the same model chemistry as geometry optimizations. The thirty lowest excited states were calculated for the doublet states of the complexes. The stick spectra were broadened using Lorentzian functions with half-width at half-maxima (HWHM) of 0.33 eV. Mulliken population analysis was

Open Access Article. Published on 22 December 2025. Downloaded on 6/9/2026 9:34:24 AM.
This article is licensed under a Creative Commons Attribution-NonCommercial 3.0 Unported Licence.

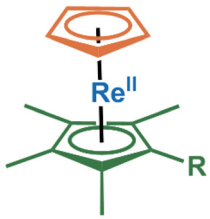


Fig. 2 Fragmentation scheme utilized to determine the localization of MOs in complexes **1–6**, where each color corresponds to a distinct fragment (orange = Cp, blue = Re, and green = $CpMe_4R$).

utilized to determine the percent compositions of MOs between the fragments using the AOMix software.[30,31] The fragmentation scheme utilized for this analysis is shown in Fig. 2.

To investigate the ground state reduction potentials of the $Re^{II/I}$ couples, the molecular geometries of the doublet states for all $ReCp(CpMe_4R)$ complexes and the singlet states for their reduced counterparts, $[ReCp(CpMe_4R)]^-$, were fully optimized. Solvent effects (THF) were included *via* a PCM.[28] Single point energy (SPE) calculations were then performed using the (U)BP86 functional[21,22] with Grimme's D3 dispersion correction for all calculated structures.[23] Ground state reduction potentials ($E^\circ$) of the $Re^{II/I}$ couple were determined relative to the ferrocenium/ferrocene ($Fc^{+/0}$) redox couple as shown in eqn (1):

$$E^\circ(\text{V } vs.\ Fc^{+/0}) = \frac{-\Delta G_{sol}}{nF} - 5.00 \quad (1)$$

where $\Delta G_{sol}$ is the change in solvated free energy upon reduction, $n$ is the number of electrons transferred in the reductive process (in this case, 1), and $F$ is Faraday's constant. The calculated reduction potentials are referenced to the $Fc^{+/0}$ couple by subtracting the reduction potential of $Fc^{+/0}$ (5.00 V *vs.* vacuum), as shown in eqn (1).[32,33] This methodology was further benchmarked utilizing $ReCp^*_2$ in THF, which was previously measured experimentally ($E^{\circ\prime}(Re^{II/I})_{exp}$ = −2.27 V *vs.* $Fc^{+/0}$),[12] and revealed good agreement within computational error ($E^\circ(Re^{II/I})_{calc}$ = −2.49 V *vs.* $Fc^{+/0}$, $\Delta E^\circ$ = 220 mV). Excited state reduction potentials for the $Re^{II*/I}$ redox couple were estimated by relating the ground state reduction potentials of the $Re^{II/I}$ redox couple to the energy stored in the LMCT excited state ($\Delta G_{ES}$), as shown in eqn (2), where $\Delta G_{ES}$ was estimated as the HOMO$\beta$–LUMO$\beta$ gap. All reduction potentials are reported *vs.* $Fc^{+/0}$.

$$E^{\circ*}(Re^{II*/I}) = E^\circ(Re^{II/I}) + \Delta G_{ES} \quad (2)$$

All calculations were carried out using the Gaussian 16 software package (Revision A.03).[34]

## Results

### Ground state electronic structure

The ground state electronic structures of six mixed-ring rhenocene derivatives were analyzed to determine the impact of functionalization on molecular orbital ordering and energetics. Optimized structures of **1–6** were obtained using unrestricted DFT. Table 1 shows the calculated distances between Re and each ring centroid ($d_{Re-Cp}$ and $d_{Re-CpMe_4R}$), average of these distances ($d_{average}$), torsion angles ($\tau$) between the Cp and $CpMe_4R$ rings, and distortion angles ($\varphi$) for each complex.

Table 1 DFT-calculated geometric parameters for $Re(Cp)(CpMe_4R)$ complexes

| Complex | $d_{Re-Cp}$ (Å) | $d_{Re-CpMe_4R}$ (Å) | $d_{average}$ (Å) | $\tau$ (°) | $\varphi$ (°) |
|---|---|---|---|---|---|
| **1** | 1.89 | 1.87 | 1.88 | 0.11 | 176 |
| **2** | 1.95 | 1.90 | 1.93 | 0.48 | 171 |
| **3** | 1.95 | 1.90 | 1.93 | 0.18 | 168 |
| **4** | 1.94 | 1.91 | 1.93 | 0.94 | 175 |
| **5** | 1.95 | 1.91 | 1.93 | 3.80 | 178 |
| **6** | 1.95 | 1.90 | 1.93 | 0.04 | 173 |

In each case, the metallocene adopts an eclipsed conformation, where the torsion angles for **1–6** are between 0.04° to 3.80° as illustrated in Fig. 3. In addition, these complexes exhibit similar Re-ring bond distances. The Re–Cp and Re–$CpMe_4R$ bond lengths of **1** are 1.89 Å and 1.87 Å, respectively. When a substituent replaces one of the methyl groups on the Cp* ligand (**2–6**), there is a slight increase in both the Re–Cp (by 0.05–0.06 Å) and Re–$CpMe_4R$ (by 0.03–0.04 Å) centroid distances. Interestingly, the Re–Cp centroid distance increases more than the Re–$CpMe_4R$ centroid distance, suggesting slightly stronger electronic interactions between the Re and substituted $CpMe_4R$ rings than Re and Cp*. Further analysis of the individual Re–C bond lengths (see Table S1 and Fig. S1) also reveals changes to the Re–C bond distances upon substitution consistent with the changes in the centroid distances. Comparison across the series reveals this distortion stems from steric encumbrance of appended substituents, where complexes with bulkier substituents (*e.g.*, **2**, **3** and **6** where R = $CF_3$ $^t$Bu, and OMe, respectively) exhibit larger distortion angles ($\varphi$) than those with smaller substituents (as highlighted in Fig. 3 and Table 1). This out-of-plane tilting allows greater electronic interaction between Re and the substituted carbon as the steric bulk of the substituent increases and shortens the Re–C bond distances. While these differences in bond lengths are small, these results suggest that steric effects directly impact the ground state electronic structures of mixed-ring rhenocenes.

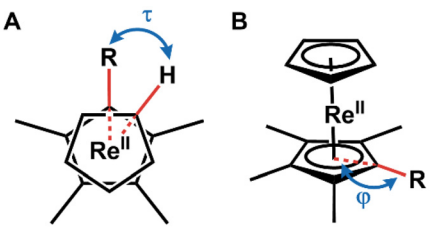


Fig. 3 Definition of the (A) torsion angle ($\tau$) and (B) distortion angle ($\varphi$) for complexes **1–3**.


This journal is © The Royal Society of Chemistry 2026

Open Access Article. Published on 22 December 2025. Downloaded on 6/9/2026 9:34:24 AM.
This article is licensed under a Creative Commons Attribution-NonCommercial 3.0 Unported Licence.

From single point energy calculations of each geometry-optimized structure, molecular orbital (MO) diagrams were constructed to determine the ground state electronic structure of each complex. Upon inspection, all complexes exhibit open shell, doublet ground states, consistent with electronic configurations known for other low-spin $d^5$ metallocenes like $ReCp^*_2$.[12,35–38] However, unlike previous reports which have largely focused on highly symmetric metallocenes (typically with $D_5$ symmetry, assuming free rotation of both Cp rings in solution), **1–6** display lower symmetry. **1** has $C_{5v}$ symmetry, resulting from the mixed ring composition, whereas **2–6** have $C_s$ symmetry that arise from additional functionalization of a single ring. As a result, the MO diagram of **1** contains three sets of d orbitals: $e_2$ ($d_{xy}$ and $d_{x^2-y^2}$), $a_1$ ($d_{z^2}$), and $e_1$ ($d_{xz}$ and $d_{yz}$) orbitals (Fig. 4). The $d_{xy}$ and $d_{x^2-y^2}$ orbitals are nearly degenerate for both α and β orbitals and the $d_{z^2}$ orbitals exhibit their own discrete energies. As such, **1** has a $^2A_1$ ground state (Fig. 5A) and the LUMOβ exhibits $d_{z^2}$ character. The ground state electronic structure of **1** differs from $ReCp^*_2$, which has a $^2E_2$ ground state and a $d_{x^2-y^2}$-based LUMOβ.[25] This change in electronic ground state may result in changes in ground state reactivity. For instance, a wide variety of metallocenes are known to undergo reactions to bind and/or activate substrates (*e.g.*, $N_2$, CO, olefins, solvent molecules, *etc.*).[39–43] In order for these chemical reactions to proceed, sufficient orbital overlap is required to promote binding and restructuring of the metallocene's geometry and, as such, the identity of frontier orbitals is critical in dictating accessible reactivity.[44,45]

In comparison, the MO diagrams of **2–6** exhibit greater complexity, resulting from their lower symmetries. Upon this descent in symmetry, the $e_1$ degeneracy of the $d_{xy}$ and $d_{x^2-y^2}$ orbitals breaks, as well as the $e_2$ degeneracy of the $d_{xz}$ and $d_{yz}$ orbitals. As such, each d orbital independently transforms with either *a′* or *a″* symmetry (Fig. 5B). This orbital splitting is reflected in the DFT-calculated MO diagrams for all five complexes (where **2** and **3** are highlighted in Fig. 4, as they are representative of the series and **4–6** are found in Fig. S2–S5). All substituted complexes (**2–6**) exhibit LUMOβs with $d_{x^2-y^2}$ character, consistent with a $^2A''$ ground state for $C_s$ complexes. These $^2A''$ electronic configurations of **2–6** are most reminiscent of the $^2E_2$ ground state of $D_5$ complexes like $ReCp^*_2$ due to their $d_{x^2-y^2}$ LUMOβ character, instead of **1** which exhibits $d_{z^2}$ LUMOβ character.

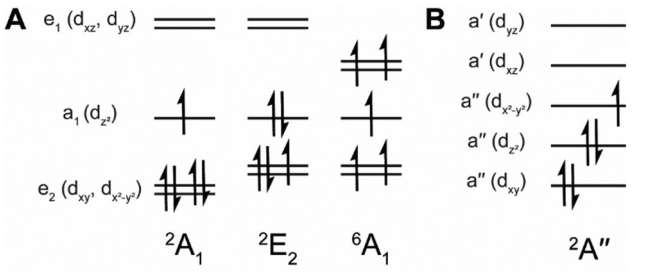


**Fig. 5** (A) Possible ground state electronic configurations for $D_5$ and $C_{5v}$ complexes. (B) One possible $^2A''$ state of $C_s$ complexes, representing the ordering calculated **2–6**. Reordering of each orbital is possible for other $C_s$ complexes and depends on orbital energetics and overlap. Term symbols are dictated by the symmetry of the LUMO orbital.

In addition to comparing the frontier orbitals of **1–6**, the impact of electron-withdrawing and electron-donating groups on absolute orbital energetics can similarly be analyzed. Appending either an electron-withdrawing trifluoromethyl or formyl group onto the mixed-ring rhenocene (**2** and **5**) results in the stabilization of both occupied and unoccupied orbitals relative to the unfunctionalized mixed rhenocene (**1**, Fig. S3). Upon addition of an electron-donating *tert*-butyl, vinyl or methoxy group (**3**, **4** and **6**), occupied orbitals are slightly stabilized relative to **1**, whereas unoccupied orbitals are destabilized (Fig. S3). Overall, these ligand substitutions result in

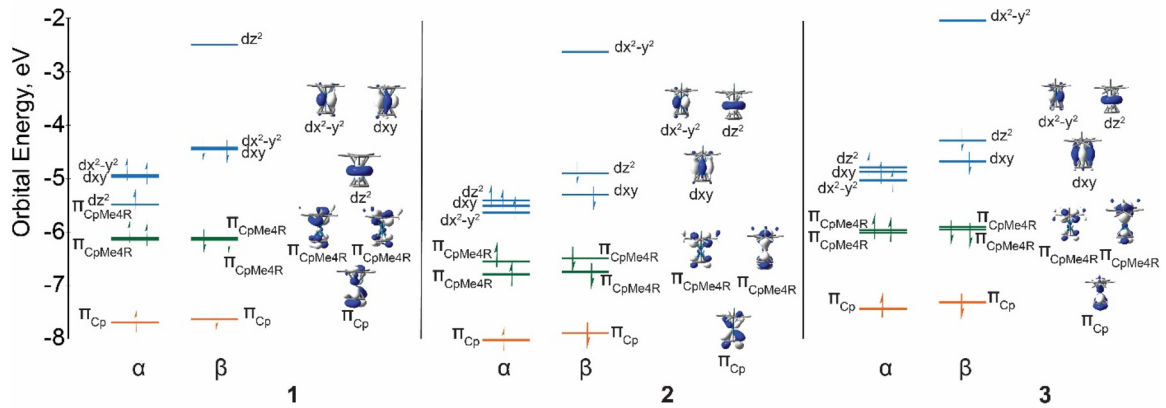


**Fig. 4** Energy level diagram of the doublet ground states of **1**, **2** and **3** using B3LYP + D2/6-311G*, SDD(Re) in benzene. MOs with >70% localization on the metal center are labeled in blue, those with >50% localization on Cp are shown in orange, and MOs with >50% localization on $CpMe_4R$ are shown in green. Please note that since all complexes are open shell, the spin-up (α) and spin-down (β) MOs are not restricted to have the same energies and occupation in the electronic structure calculations (as is typically done for closed shell molecules) in order to find the lowest-energy electronic state. Also note that $d_{xz}$ and $d_{yz}$ orbitals are unoccupied for all complexes and lie higher in energy, outside of the energy window chosen for plotting.

Open Access Article. Published on 22 December 2025. Downloaded on 6/9/2026 9:34:24 AM.
This article is licensed under a Creative Commons Attribution-NonCommercial 3.0 Unported Licence.

higher HOMO$\beta$–LUMO$\beta$ gaps of complexes **2–6** than complex **1**, (Fig. S6) and should result in a hypsochromic shift of the LMCT excited state in their UV-Vis absorption spectra, regardless of the ligand donating or withdrawing ability of the substituent.

### UV-Vis absorption spectra

Guided by the impact of ligand substitution on HOMOβ and LUMOβ energies, the UV-Vis absorption spectra for **1–6** were calculated using TD-DFT methods to assess analogous trends in the photophysical properties of mixed-ring rhenocenes. In general, these complexes exhibit similar absorption profiles with a single low energy feature centered at ~450–500 nm and a more intense absorption feature in the ultraviolet region, as shown by the stick spectra overlaid with the calculated absorption spectra (Fig. 6). For **1**, this low energy feature is comprised of two near-degenerate electronic transitions centered at 518 nm with oscillator strengths ($f$) of ~0.003. Similarly, both electronic transitions display 99% LMCT character, where the π orbitals of both Cp ligands (HOMO−3β and HOMO−2β) donate to the Re $d_{z^2}$ orbital (LUMOβ), consistent with previous reports of $ReCp^*_2$.[12] Fig. 7 shows the transitions of the lowest excited states of complexes **1–3**. The lowest excited states for complexes **4–6** are shown in Fig. S7. For the electron-withdrawing derivatives (**2** and **5**), appending trifluoromethyl and formyl groups to the mixed-ring rhenocene results in a hypsochromic shift of both LMCT transitions (462 nm and 424 nm for **2** and 476 nm and 439 nm for **5**). As expected, these transitions are no longer degenerate, reflecting the descent in symmetry of **1** ($C_{5v}$) to **2** and **5** ($C_s$). Likewise, their hypsochromic shifts result from the greater stabilization of the donor π orbitals (HOMO−4β, HOMO−3β and HOMO−2β) than the acceptor Re $d_{x^2-y^2}$ orbital (LUMOβ), as highlighted above. Both LMCT transitions also exhibit slightly higher oscillator strengths than **1** ($f \sim 0.01$ for both transitions in **2** and $f \sim 0.009$ for both transition in **5**) and analogous LMCT character (98%–99% LMCT character) compared to **1**. The slight increase in oscillator strength can be attributed to greater orbital overlap between the hole–particle orbitals in **2** and **5** than in **1**. As shown in Fig. 7 and Fig. S6, the $d_{x^2-y^2}$ orbital is populated upon low-energy excitation of **2** and **5**, instead of the $d_{z^2}$ orbital in **1**. The $d_{x^2-y^2}$ orbital exhibits greater interaction with Cp and $CpMe_4R$ ring π systems than $d_{z^2}$, leading to greater orbital overlap with the ligand-localized p orbitals from which the electron is transferred.

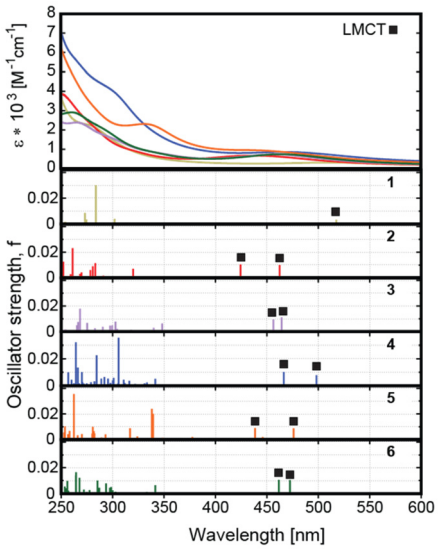


**Fig. 6** Calculated UV-Vis absorption spectra of **1–6**.

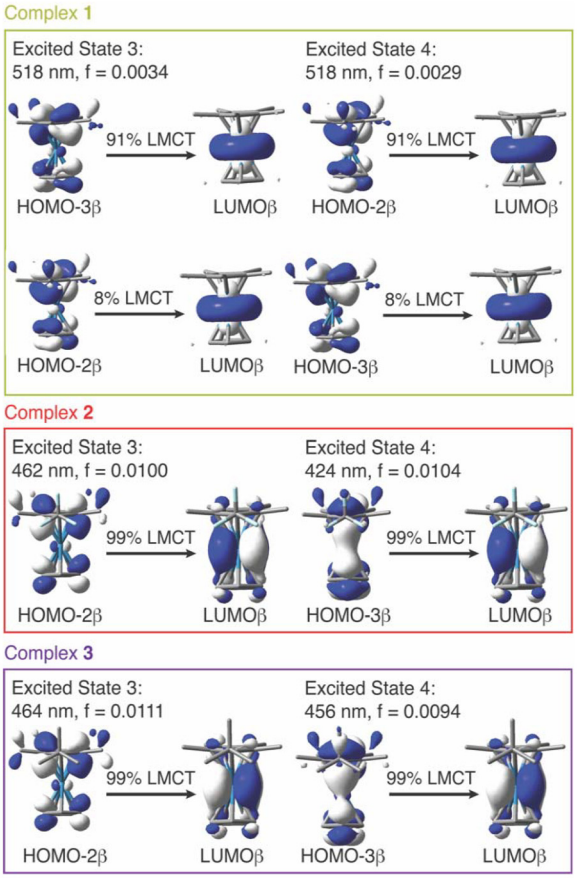


**Fig. 7** Donor and acceptor orbitals of the lowest energy excited states for complexes **1–3**. Calculated excitation energies (in nm) and oscillator strengths ($f$) for each electronic transition are provided. The percent contribution of the displayed hole-particle pair determined from the excitation coefficients obtained from the TD-DFT calculations is also provided.

Similar results were found for the electron-donating derivatives (**3**, **4** and **6**). Their LMCT excited states are also hypsochromically shifted (centered at 464 nm and 456 nm; $f \sim 0.01$ for both transitions in **3**, 498 nm and 466 nm; $f \sim 0.008$ and 0.01 respectively for **4** and 473 nm and 462 nm; $f \sim 0.01$ for both transitions in **6**) and exhibit similar LMCT character (98%–99% each) compared to **1**. Furthermore, the oscillator strengths for **3**, **4** and **6** are similar to **2** and **5**, owing to its analogous population of the $d_{x^2-y^2}$ orbital in the excited state. Overall, these results suggest that the functionalization of


This journal is © The Royal Society of Chemistry 2026

Open Access Article. Published on 22 December 2025. Downloaded on 6/9/2026 9:34:24 AM. This article is licensed under a Creative Commons Attribution-NonCommercial 3.0 Unported Licence.

mixed-ring rhenocenes conserves the LMCT character of its low-lying electronic transitions.

## Ground and excited state reduction potentials

Upon discovering that ligand electronics tune both HOMOβ and LUMOβ orbital energies, we hypothesized ligand functionalization may also serve to control reduction potentials. Using optimized geometries of all ReCp(CpMe$_4$R) complexes and their respective reduced species, [ReCp(CpMe$_4$R)]$^-$, single point energy calculations were conducted and utilized to estimate the reduction potentials of each $Re^{II/I}$ couple *vs.* $Fc^{+/0}$ of **1–6**, as shown in eqn (1) and reported in Table 2. Calculations were benchmarked using the reduction potential of the [ReCp$^*_2$]$^{0/-}$ redox couple which has been previously measured experimentally ($E^{\circ\prime}(Re^{II/I})_{exp}$ = −2.27 V *vs.* $Fc^{+/0}$ in THF).[12] The calculated reduction potential ($E^{\circ}(Re^{II/I})_{calc}$ = −2.49 V *vs.* $Fc^{+/0}$) showed good agreement with the experimental value (*i.e.*, within 220 mV), showcasing the efficacy of this methodology.

Across this suite of complexes, the reduction potential of the $Re^{II/I}$ couple varied over 400 mV as a function of ligand donor ability. Complexes with greater donor ability (*e.g.*, **6** where R = OMe) exhibited the most negative reduction potentials, whereas those with electron withdrawing ability exhibited more positive reduction potentials (*e.g.*, **5** where R = CHO). When ordered with respect to their ligand donor strength (**6** > **3** ∼ **1** > **4** > **2** > **5**, where OMe > $^t$Bu ∼ Me > $CHCH_2$ > $CF_3$ > CHO) and compared directly to their reduction potentials, this trend is further highlighted, where reduction potentials are ordered as follows **1** < **3** < **6** < **4** < **2** < **5**. However, it is important to note slight deviations from the anticipated and observed trends, where the ordering of complexes bearing electron donating groups does not directly trend with donor strength (albeit within 90 mV). This deviation may be attributed to the difference in molecular symmetry of **1** ($C_{5v}$) and/or the inherent error within the theoretical methodology. Nonetheless, this approach highlights that small changes in molecular structure can vary the reduction potential of heteroleptic rhenocenes over a range of 400 mV.

Upon determining the ground state reduction potentials of all [ReCp(CpMe$_4$R)]$^{0/-}$ couples, excited state reduction potentials ($E^{\circ *}$) for the $Re^{II*/I}$ redox couple were similarly calculated to assess the impact of ligand substitution on the photophysical properties of these complexes. These values were computed utilizing the ground state reduction potentials ($E^{\circ}$) and energy stored in the LMCT excited states ($\Delta G_{ES}$, estimated as the computed HOMO$\beta$–LUMO$\beta$ gaps), as summarized in Table 2 (see eqn (2) in Methodology for calculation details). Excited state reduction potentials ($E^{\circ *}$) were found to span 720 mV, where **5** exhibited the most photo-oxidizing potential ($E^{\circ *}(Re^{II*/I})$ = 0.52 V *vs.* $Fc^{+/0}$) and **1** exhibited the least photo-oxidizing potential ($E^{\circ *}(Re^{II*/I})$ = −0.20 V *vs.* $Fc^{+/0}$). However, it is important to note that these calculated $E^{\circ *}(Re^{II*/I})$ are likely overestimated compared to experimental data, as the experimental $\Delta G_{ES}$ are typically estimated conservatively as the crossing point of UV-vis absorption and photoluminescence spectra. This analysis is further highlighted *via* the benchmarking of ReCp$^*_2$, where the computed HOMO$\beta$–LUMO$\beta$ gap (an estimate of $\Delta G_{ES}$) was 2.45 eV and the experimentally determined $\Delta G_{ES}$ was 2.07 eV.[12]

Regardless, these calculations highlight that complexes **2–6** should exhibit greater potency as photo-oxidants, largely owing to the hypsochromic shift of their LMCT excited states and concomitant increase in $\Delta G_{ES}$ for lower symmetry complexes (**2–6**) compared to **1**. Additional fine tuning to more positive potentials is possible by appending electron withdrawing groups, generating even greater potency as photo-oxidants (*e.g.*, **2** and **5**). These structural modifications tune the ground state reduction potentials to more positive potentials, and in turn, result in more positive excited state reduction potentials for the $Re^{II*/I}$ couples. Collectively, these results showcase synthetic routes to tune the potency of the LMCT excited states of mixed-ring rhenocenes, whereupon modifying rhenocene geometry and ligand identity play key roles in modulating ground state electronic structure, LMCT energies, and reduction potentials to curate tailored rhenocenes poised for photochemical applications.

**Table 2** Redox potentials for the six complexes investigated calculated at the BP86+D3/SDD,6-311G* in THF based on B3LYP+D3/SDD,6-311G* optimized structures

| Complex | $E^{\circ}$ ($Re^{II/I}$) [V *vs.* $Fc^{+/0}$] | $\Delta G_{ES}$ [eV] | $E^{\circ *}$ ($Re^{II*/I}$) [V *vs.* $Fc^{+/0}$] |
|---|---|---|---|
| **1** | −2.14 | 1.94 | −0.20 |
| **2** | −1.84 | 2.27 | 0.43 |
| **3** | −2.10 | 2.25 | 0.15 |
| **4** | −1.97 | 2.21 | 0.24 |
| **5** | −1.71 | 2.23 | 0.52 |
| **6** | −2.05 | 2.27 | 0.22 |

## Conclusions

In this study, the impact of molecular symmetry and ligand donation on the ground state electronic structure and excited state properties of six mixed-ring rhenocenes were investigated. Overall, we found that changes in the electronic structure drive the photochemical reactivity and potency of excited states. Geometry optimizations revealed eclipsed geometries for all mixed-ring rhenocene complexes. Subtle changes in the bond distances indicate distortion to a lower symmetry (from $C_{5v}$ to $C_s$) upon the addition of substituents to the Cp* ring and suggest steric bulk contributes marginally to the ground state electronic structure. DFT calculations suggest that **1** exhibits a $^2A_1$ ground state where the LUMOβ exhibits $d_{z^2}$ character, whereas the lower symmetry complexes, **2–6**, exhibit $^2A''$ ground states with LUMOβs that exhibit $d_{x^2-y^2}$ character. Inspection of the absolute energetics of the molecular orbitals revealed that appending electron-withdrawing substituents (**2**

Open Access Article. Published on 22 December 2025. Downloaded on 6/9/2026 9:34:24 AM.
This article is licensed under a Creative Commons Attribution-NonCommercial 3.0 Unported Licence.

and **5**) stabilized both occupied and unoccupied MOs compared to unfunctionalized **1**. Conversely, electron-withdrawing groups slightly stabilized occupied orbitals, but destabilized unoccupied orbitals (**3**, **4**, and **6**).

TD-DFT calculations were then employed to simulate the UV-vis absorption profiles and accompanying fragment orbital analysis enabled the assignment of the low energy absorption features to LMCT, consistent with reports for other rhenocene derivatives. These results support that the LMCT character of low energy electronic transitions is maintained regardless of molecular symmetry and the presence of electron-donating or electron-withdrawing groups. However, while the character of these low-energy transitions is conserved, their energies and oscillator strengths are impacted. In particular, **2–6** are hypsochromically shifted compared to **1** and higher oscillator strengths for these transitions are observed, resulting from changes in HOMO$\beta$–LUMO$\beta$ gaps and the nature of the orbital being occupied upon excitation due to the impact of the substituent groups on the electronic structure of the complexes.

Upon examining trends in ground state electronic structure and photophysical properties, the ground and excited state reduction potentials for the $Re^{II/I}$ and $Re^{II*/I}$ redox couples, respectively, were calculated. Ground state reduction potentials ranged −1.71 V to −2.14 V *vs.* $Fc^{+/0}$, spanning over 400 mV. In general, reduction potentials trended with electron donating ability of the substituted ligands, where electron-donating substituents promoted more negative reduction potentials, whereas electron-withdrawing substituents shifted reduction potentials to more positive potentials. Utilizing these calculated ground state reduction potentials and the energies stored in the LMCT excited states, excited state reduction potentials for the $Re^{II*/I}$ couple were also calculated, showcasing similar tunability over 700 mV and access to stronger photo-oxidants compared to previously reported $ReCp^*_2$. This tunability depends on the hypsochromic shift observed for **2–6** compared to **1**, as well as the impact of ligand substituent on ground state reduction potentials. Together, these data illustrate how the intricate relationships between molecular symmetry and ligand electronics impact the ground and excited electronic structure, thereby enabling the tailored design of next generation rhenocene derivatives for photochemical applications.

## Conflicts of interest

There are no conflicts to declare.

## Data availability

Supplementary information is available. Frontier MOs, results of FO analysis, and the excited-state characterization for all complexes studied can be found in a PDF file. Cartesian coordinates for DFT-optimized structures of all complexes in their doubled ground states are provided as an XYZ file. See DOI: https://doi.org/10.1039/d4dt03309d.

## Acknowledgements

This work was supported by the National Science Foundation (CHE-1954868 and CHE-2400727). A. M. M. acknowledges support from the Department of Defense *via* a National Defense Science and Engineering Graduate fellowship. E. J., G. C. and E. A. gratefully acknowledge the Department of Chemistry at NCSU for funding. We also acknowledge the use of the computing resources provided by North Carolina State University High Performance Computing Services Core Facility (RRID: SCR 022168).

## References

1 N. S. Kochetkova, M.-G. A. Shvekhgeimer and L. V. Balabanova, *Russ. Chem. Rev.*, 1984, **53**, 1168.
2 Y. Yamaguchi, W. Ding, C. T. Sanderson, M. L. Borden, M. J. Morgan and C. Kutal, *Coord. Chem. Rev.*, 2007, **251**, 515–524.
3 K. V. Prather and E. Y. Tsui, *Inorg. Chem.*, 2023, **62**, 2128–2134.
4 E. K. Heaney, S. R. Logan and W. E. Watts, *J. Organomet. Chem.*, 1978, **150**, 309–319.
5 R. E. Bozak, in *Advances in Photochemistry*, John Wiley & Sons, Ltd, 1971, pp. 227–244.
6 E. Román, M. Barrera, S. Hernández and E. Lissi, *J. Chem. Soc., Perkin Trans. 2*, 1988, 939–942.
7 R. W. Harrigan, G. S. Hammond and H. B. Gray, *J. Organomet. Chem.*, 1974, **81**, 79–85.
8 J. J. Dannenberg and J. H. Richards, *J. Am. Chem. Soc.*, 1965, **87**, 1626–1627.
9 F. Dumur, *Eur. Polym. J.*, 2021, **147**, 110328.
10 R. Sievers, J. Parche, G. N. Kubi and M. Malischewski, *Synlett*, 2023, 1079–1086.
11 R. Sievers, M. Sellin, S. M. Rupf, J. Parche and M. Malischewski, *Angew. Chem., Int. Ed.*, 2022, e202211147.
12 A. M. May, M. Deegbey, K. Edme, K. J. Lee, R. N. Perutz, E. Jakubikova and J. L. Dempsey, *Inorg. Chem.*, 2024, **63**, 1858–1866.
13 J. N. Hill, R. N. Perutz and S. M. Tavender, *J. Phys. Chem.*, 1996, **100**, 934–940.
14 F. G. N. Cloke and J. P. Day, *J. Chem. Soc., Chem. Commun.*, 1985, 967–968.
15 F. G. N. Cloke, J. P. Day, J. C. Green, C. P. Morley and A. C. Swain, *J. Chem. Soc., Dalton Trans.*, 1991, 789–796.
16 J. A. Bandy, F. G. N. Cloke, G. Copper, J. P. Day, R. B. Girling, R. G. Graham, J. C. Green, R. Grinter and R. N. Perutz, *J. Am. Chem. Soc.*, 1988, **110**, 5039–5050.
17 R. A. Paciella, P. Kiprof, E. Herdtweck and W. A. Herrmann, *Inorg. Chem.*, 1989, **28**, 2890–2893.
18 H.-J. Zhang, B. Demerseman, Z. Xi and C. Bruneau, *Eur. J. Inorg. Chem.*, 2008, 3212–3217.
19 B. Dutta, E. Solari, S. Gauthier, R. Scopelliti and K. Severin, *Organometallics*, 2007, **26**, 4791–4799.


This journal is © The Royal Society of Chemistry 2026

Open Access Article. Published on 22 December 2025. Downloaded on 6/9/2026 9:34:24 AM. This article is licensed under a Creative Commons Attribution-NonCommercial 3.0 Unported Licence.

20 M. Sato, Y. Kawata, A. Kudo, A. Iwai, H. Saitoh and S. Ochiai, *J. Chem. Soc., Dalton Trans.*, 1998, 2215–2224.
21 (*a*) A. D. Becke, *Phys. Rev. A*, 1988, **38**, 3098–3100; (*b*) J. P. Perdew, *Phys. Rev. A*, 1986, **33**, 8822–8824.
22 (*a*) A. D. Becke, *J. Chem. Phys.*, 1993, **98**, 1372–1377; (*b*) C. Lee, W. Yang and G. R. Parr, *Phys. Rev. B: Condens. Matter Mater. Phys.*, 1988, **37**, 785–789; (*c*) H. S. Vosko, L. Wilk and M. Nusair, *Can. J. Phys.*, 1980, **58**, 1200–1211.
23 S. Grimme, J. Antony, S. Ehrlich and H. Krieg, *J. Chem. Phys.*, 2010, **132**, 154104.
24 M. Kaupp, P. V. R. Schleyer, H. Stoll and H. Preuss, *J. Chem. Phys.*, 1991, **94**, 1360–1366.
25 A. W. Ehlers, M. Böhme, S. Dapprich, A. Gobbi, A. Höllwarth, V. Jonas, K. F. Köhler, R. Stegmann, A. Veldkamp and G. Frenking, *Chem. Phys. Lett.*, 1993, **208**, 111–114.
26 R. Krishnan, J. S. Binkley, R. Seeger and J. Pople, *J. Chem. Phys.*, 1980, **72**, 650–654.
27 A. D. McLean and G. S. Chandler, *J. Chem. Phys.*, 1980, **72**, 5639–5648.
28 G. Scalmani and M. J. Frisch, *J. Chem. Phys.*, 2010, **132**, 114110.
29 M. E. Casida, C. Jamorski, K. C. Casida and D. R. Salahub, *J. Chem. Phys.*, 1998, **108**, 4439–4449.
30 S. I. Gorelsky and A. B. P. Lever, *J. Organomet. Chem.*, 2001, **635**, 187–196.
31 S. I. Gorelsky, *AOMix Program, ver. 6.94b*, 2023.
32 R. R. Gagne, C. A. Koval and G. C. Lisensky, *Inorg. Chem.*, 1980, **19**, 2854–2855.
33 H. M. Koepp, H. Wendt and H. Stkehlow, *Z. Elektrochem., Ber. Buns. Phys. Chem.*, 1960, **64**, 483–491.
34 M. J. Frisch, G. W. Trucks, H. B. Schlegel, G. E. Scuseria, M. A. Robb, J. R. Cheeseman, G. Scalmani, V. Barone, G. A. Petersson, H. Nakatsuji, X. Li, M. Caricato, A. V. Marenich, J. Bloino, B. G. Janesko, R. Gomperts, B. Mennucci, H. P. Hratchian, J. V. Ortiz, A. F. Izmaylov, J. L. Sonnenberg, D. Williams-Young, F. Ding, F. Lipparini, F. Egidi, J. Goings, B. Peng, A. Petrone, T. Henderson, D. Ranasinghe, V. G. Zakrzewski, J. Gao, N. Rega, G. Zheng, W. Liang, M. Hada, M. Ehara, K. Toyota, R. Fukuda, J. Hasegawa, M. Ishida, T. Nakajima, Y. Honda, O. Kitao, H. Nakai, T. Vreven, K. Throssell, J. A. Montgomery Jr., J. E. Peralta, F. Ogliaro, M. J. Bearpark, J. J. Heyd, E. N. Brothers, K. N. Kudin, V. N. Staroverov, T. A. Keith, R. Kobayashi, J. Normand, K. Raghavachari, A. P. Rendell, J. C. Burant, S. S. Iyengar, J. Tomasi, M. Cossi, J. M. Millam, M. Klene, C. Adamo, R. Cammi, J. W. Ochterski, R. L. Martin, K. Morokuma, O. Farkas, J. B. Foresman and D. J. Fox, *Gaussian 16 Rev. C.01*, 2016.
35 J. H. Ammeter, R. Bucher and N. Oswald, *J. Am. Chem. Soc.*, 1974, **96**, 7833–7835.
36 J. A. Bandy, F. G. N. Cloke, G. Copper, J. P. Day, R. B. Girling, R. G. Graham, J. C. Green, R. Grinter and R. N. Perutz, *J. Am. Chem. Soc.*, 1988, **110**, 5039–5050.
37 H. B. Gray, Y. S. Sohn and N. Hendrickson, *J. Am. Chem. Soc.*, 1971, **93**, 3603–3612.
38 F. G. N. Cloke, A. N. Dix, J. C. Green, R. N. Perutz and E. A. Seddon, *Organometallics*, 1983, **2**, 1150–1159.
39 T. E. Hanna, E. Lobkovsky and P. J. Chirik, *J. Am. Chem. Soc.*, 2004, **126**, 14688–14689.
40 T. E. Hanna, E. Lobkovsky and P. J. Chirik, *J. Am. Chem. Soc.*, 2006, **128**, 6018–6019.
41 R. H. Grubbs and G. W. Coates, *Acc. Chem. Res.*, 1996, **29**, 85–93.
42 L. Rivier, T. J. Stockmann, M. A. Méndez, M. D. Scanlon, P. Peljo, M. Opallo and H. H. Girault, *J. Phys. Chem. C*, 2015, **119**, 25761–25769.
43 C. Magnoux and D. P. Mills, *Eur. J. Inorg. Chem.*, 2022, **2022**, e202101063.
44 C. J. Green, *Chem. Soc. Rev.*, 1998, **27**, 263–272.
45 J. W. Lauher and R. Hoffmann, *J. Am. Chem. Soc.*, 1976, **98**, 1729–1742.